Correlated N/O anion orders in melilite phosphors

Correlated N/O anion orders in melilite phosphors

Paula Kayser[a], Hannah E. Johnston[a], Mu- Hai Fang[b], David A. Keen[c], Ru Shi Liu[b,*] and J. Paul Attfield[a,*]

[a] CSEC and School of Chemistry, University of Edinburgh, King's Buildings, Mayfield Road, Edinburgh, EH9 3JZ, U.K.

[b] Department of Chemistry, National Taiwan University, No. 1, Sec. 4, Roosevelt Road, Taipei 106, Taiwan

[c] ISIS Facility, Rutherford Appleton Laboratory, Didcot, OX11 0QX, U.K.

Abstract

The N/O anion distributions in the melilite-type phosphor host material $Y_2Si_3O_3N_4$ and a Ce-doped sample $Y_{1.5}Ce_{0.5}Si_3O_3N_4$ have been determined from powder neutron diffraction. Both materials have a highly ordered N/O distribution that is not changed significantly by the disorder introduced by Ce doping. This distribution evidences the presence of SiN_3O and SiN_2O_2 tetrahedra and although these are not fully long range-ordered, local structural correlations follow simple connectivity rules that lead to an estimated residual molar entropy of R ln3. A broad range of N/O environments is found around 8-coordinate Y(Ce) sites which is expected to broaden their spectroscopic features.

Corresponding authors:

e-mails: Ru-Shi Liu (rsliu@ntu.edu.tw) and J.P. Attfield (j.p.attfield@ed.ac.uk)

1. Introduction

In recent decades, there has been a great development of new materials containing more than one anion, such as oxyfluorides, oxynitrides and oxyhydrides, which may combine the benefits of the two anions. This emerging area of mixed-anion compounds provides a novel field of solid-state chemistry to explore [1]. Conventional solid-state chemistry reactions are often not adequate for these materials and alternative synthetic procedures such as ammonolysis, topochemical insertion and exchange reactions or high-pressure techniques are required. Regarding the crystal structure, there is an additional challenge that involves the investigation of the long-range and local anion ordering, which may be important to understand and ultimately tailor the physical properties.

Metal oxynitrides [2, 3] have been intensively studied due to their great potential as phosphors, photocatalysts, dielectric and magnetic materials. The substitution of nitride, a less electronegative and

more polarizable anion than oxide, increases the covalency of bonding and the expansion of the electron cloud while decreasing the interelectronic repulsions. The higher charge of the nitride anion allows transition metal materials with higher oxidation states cations to be stabilised and gives rise to a larger crystal field splitting that may lead to substantial changes in optical properties [4]. Among luminescent materials, silicon nitrides and oxynitrides [5-8] have been widely studied due to their excellent properties: low toxicity, good thermal stability, and great colour tunability. Particularly interesting are Ce^{3+} or Eu^{2+} activated oxynitridesilicate phosphors, which represent a family of luminescent compounds with long wavelengths and broad emission bands. Y-Si-O-N systems are efficient host lattices for luminescent materials and the substitution of Y^{3+} by Ce^{3+} leads to 5d→4f emission in the near-ultraviolet or blue region. $Y_2Si_3O_3N_4:Ce^{3+}$ is a phosphor that shows intense absorption in the near-ultraviolet region and exhibits bright blue emission and so is a promising blue-emitting phosphor candidate for white LEDs for general illumination or displays. [9,10]

$Y_2Si_3O_3N_4$ has the melilite type crystal structure [11-15], which crystallises in the tetragonal $P\bar{4}2_1m$ space group. There is a unique site for Y, two different crystallographic sites for the Si atoms, and three different anion sites. Since local crystal structure has a strong impact on the emission and excitation spectra of these cations, we have studied here the order of the N/O anions in $Y_2Si_3O_3N_4$, and in a heavily doped $Y_{1.5}Ce_{0.5}Si_3O_3N_4$ sample to discover whether the Y/Ce cation disorder has any effects on the anion ordering.

2. Experimental Methods

Polycrystalline $Y_2Si_3O_3N_4$ and $Y_{1.5}Ce_{0.5}Si_3O_3N_4$ samples were prepared by high-temperature solid-state reaction. Stoichiometric quantities of Y_2O_3 (Aldrich, 99.9%), CeO_2 (Aldrich, 99.995%), and α-Si_3N_4 (Aldrich, 99.6%), were weighed and ground in an agate mortar for 30 minutes, transferred into molybdenum crucibles and placed in a tube furnace. The precursors were heated at 5 °C min^{-1} up to 1700 °C and sintered for 2 h under a reducing and nitriding atmosphere of 5%/95% H_2/N_2 gas.

Time-of-flight powder neutron diffraction data from both samples were collected at room temperature using the diffractometer GEM at the ISIS facility, UK. The profile fits via the Rietveld method [16] were carried out using the FullProf software package [17]. A pseudo-Voigt function convoluted with an Ikeda-Carpenter function was used to generate the line shape of the peaks, and the background was fitted using linear interpolation. The following parameters were refined in the final runs together with the peak shape parameters: scale factor, detector zero-point, lattice parameters, atomic coordinates and isotropic atomic displacement (*B*) parameters.

3. Results

Both samples were found to have melilite-type structures and neutron diffraction peaks were indexed with tetragonal space group $P\bar{4}2_1m$. Y/Ce atoms are located at 4e sites (x, x+1/2, z) and Si atoms have two Wyckoff positions, Si1 at 4e sites (x, x+1/2, z) and Si2 at 2a sites (0,0,0). The anions are distributed over three sites; 2c (1/2, 0,z), 4e (x, x+1/2, z) and 8f (x,y,z) and the high neutron contrast between O and N (scattering lengths 5.80 and 9.36 fm, respectively) enabled their site occupancies to be independently varied in initial refinements, as shown in Table 1.

Table 1. N/O anion site occupancies (%) for $Y_2Si_3O_3N_4$ and $Y_{1.5}Ce_{0.5}Si_3O_3N_4$ from initial Rietveld fits.

Site	$Y_2Si_3O_3N_4$	$Y_{1.5}Ce_{0.5}Si_3O_3N_4$
$(N/O)_{2c}$	92/8(2)	92/8(4)
$(N/O)_{4e}$	8/92(4)	4/96(2)
$(N/O)_{8f}$	74/26(1)	75/25(4)

These results show that the N/O distribution is highly ordered and is not changed significantly by the cation disorder introduced by Ce doping. Based on these results, we have assumed that the site 2c is entirely occupied by nitrogen and the position 4e with oxygen, while the 8f presents a mixed N/O occupancy with 3:1 ratio in the final refinement model. These assumptions do not significantly change the fitting residuals ($Y_2Si_3O_3N_4$: residuals R_{wp}= 5.37/5.36 % and R_F= 2.87/2.87 %, and $Y_{1.5}Ce_{0.5}Si_3O_3N_4$: R_{wp}= = 6.66/6.60 % and R_F= 2.25/2.23 % for the refined-/fixed- occupancy models). The refined parameters are shown in Table 2 and selected bond distances and angles are displayed in Table 3. Good agreement between the experimental and calculated points is seen in the profile fits in Figure 1, and a view of the melilite structure showing the average anion occupancies is in Figure 2.

Table 2. Final Rietveld refined values of cell parameters, atomic coordinates and isotropic thermal parameters for $Y_2Si_3O_3N_4$ and $Y_{1.5}Ce_{0.5}Si_3O_3N_4$ defined in the space group $P\bar{4}2_1m$, from powder neutron data at room temperature.

		$Y_2Si_3O_3N_4$	$Y_{1.5}Ce_{0.5}Si_3O_3N_4$
	a (Å)	7.5991(5)	7.6425(3)
	c (Å)	4.9113(4)	4.9489(3)
	V (Å^3)	283.61(3)	289.05(2)
Y/Ce 4*e* (x,x+1/2,z)	B (Å^2)	0.90(9)	0.84(8)
	x	0.3369(4)	0.3356(4)
	z	0.5041(9)	0.5045(8)
Si1 4*e* (x,x+1/2,z)	B (Å^2)	0.3(1)	0.5(1)
	x	0.1426(8)	0.1438(7)
	z	0.9495(14)	0.9514(12)
Si2 2*a* (0 0 0)	B (Å^2)	0.3(2)	0.5(2)
N 2*c* (1/2, 0,z)	B (Å^2)	0.9(1)	1.3(1)
	z	0.1883(13)	0.1844(11)
O **4*e* (x,x+1/2,z)**	B (Å^2)	0.6(1)	0.8(1)
	x	0.1404(5)	0.1403(4)
	z	0.2799(11)	0.2774(10)
N/O 8*f* (x, y,z)	B (Å^2)	0.70(8)	0.80(6)
	x	0.0871(3)	0.0858(3)
	y	0.1609(4)	0.1617(3)
	z	0.7974(7)	0.8006(6)
	Occ	0.75/0.25	0.75/0.25

Table 3. Selected interatomic distances (Å) and angles (°) for $Y_2Si_3O_3N_4$ and $Y_{1.5}Ce_{0.5}Si_3O_3N_4$ determined from powder neutron data at room temperature.

	$Y_2Si_3O_3N_4$	$Y_{1.5}Ce_{0.5}Si_3O_3N_4$
Y/Ce-N_{2c} (x1)	2.340(6)	2.380(5)
Y/Ce-O_{4e} (x2)	2.544(5)	2.573(5)
Y/Ce-O_{4e} (x1)	2.382(5)	2.391(5)
Y/Ce-$(N/O)_{8f}$ (x2)	2.383(5)	2.407(4)
Y/Ce-$(N/O)_{8f}$ (x2)	2.756(5)	2.775(4)
Si1-O_{4e} (x1)	1.623(9)	1.614(8)
Si1-N_{2c} (x1)	1.675(7)	1.693(6)
Si1-$(N/O)_{8f}$ (x2)	1.722(7)	1.721(6)
Si2-$(N/O)_{8f}$ (x4)	1.710(3)	1.712(3)
(N_{2c})-(Si1)-(O_{8f})	103.1(4)	102.8(3)
(O_{8f})-(Si1)-(O_{4e})	116.1(5)	116.3(5)
(O_{8f})-(Si1)-(N_{8f})	103.7(4)	104.9(3)
(N_{2c})-(Si1)-(O_{4e})	113.0(6)	112.0(5)
(O_{8f})-(Si2)-(O_{8f})	109.8(3)	109.4(2)

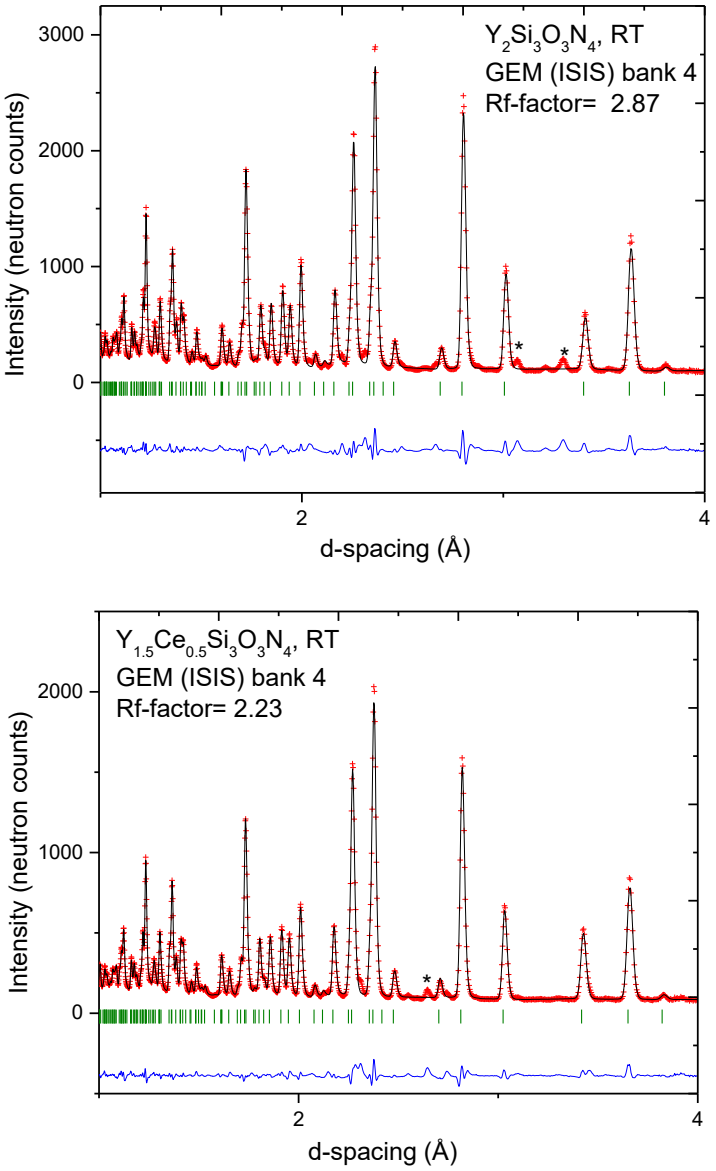

Figure 1. Observed (crosses), calculated (solid line) and difference (bottom) neutron Rietveld profiles for $Y_2Si_3O_3N_4$ (top) and $Y_{1.5}Ce_{0.5}Si_3O_3N_4$ (bottom) at room temperature, collected at the powder diffractometer GEM at ISIS. The green vertical lines indicate the positions of melilite Bragg reflections and those marked * correspond to unknown impurities.

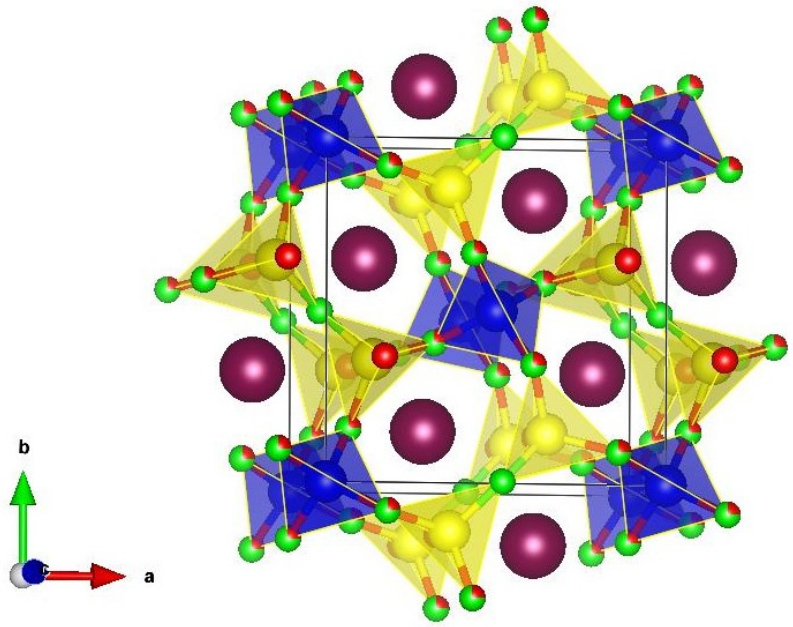

Figure 2. Schematic view of the melilite type structures of $Y_2Si_3O_3N_4$ and $Y_{1.5}Ce_{0.5}Si_3O_3N_4$ showing $Si1_2(N,O)_7$ disilicate groups in yellow and $Si2(N,O)_4$ tetrahedra in blue. N/O = green/red.

The refined unit-cell parameters of both compounds, displayed in Table 1, correlate with the sizes of the cations Y^{3+} and Ce^{3+} (1.019 Å and 1.143 Å respectively) [18]. The Ce- doped samples undergo a volume increase of 2% with a slightly larger increment along the c-axis compare to the a-axis (0.8% vs 0.6%). As shown in Figures 2 and 3, there are two types of silicon tetrahedra. Si1 is coordinated to one terminal O_{4e}, two $(N/O)_{8f}$ sites shared with Si2's, and one N_{2c} bridging to another Si1. Hence these sites may be described as forming $Si1_2(N,O)_7$ disilicate-type groups. Si1-O_{4e} distances are short (1.62/1.61 Å for $Y_2Si_3O_3N_4$/$Y_{1.5}Ce_{0.5}Si_3O_3N_4$) while Si1-$N_{2c}$ = 1.68/1.69 Å are longer reflecting the respective terminal and bridging natures of these anions and their sizes. Si1-$(N/O)_{8f}$ = 1.72/1.72 Å distances are even longer due to the anion disorder at the 8f site. Si2 atoms are coordinated to four $(N/O)_{8f}$ sites, each bridging to a Si1, and the relatively long bond Si2-$(N/O)_{8f}$ = 1.71/1.71 Å distances again reflect the site disorder. These bond distances compare well with predicted values from Shannon's [18] effective ionic radii (<Si-O_{4e}>=1.64 Å, <Si-N_{2c}>=1.72 and <Si-O,N_{8f}>=1.70 Å), with slight contractions of the distances to fully ordered N_{2c} and O_{4e} sites and a subtle expansion of distances to disordered $(N/O)_{8f}$. The rare-earth ions have an 8-coordinate polyhedral environment with five symmetry inequivalent bond distances (Table 3). The bond distances of both compounds follow the same trend with respect to the theoretical values: <Y-N_{2c}>=2.479 Å, <Y-O_{4e}>=2.399 Å, and <Y-O,N_{8f}>=2.459 Å for the undoped compounds and <$Y_{1.5}Ce_{0.5}$-N_{2c}>=2.510 Å, < $Y_{1.5}Ce_{0.5}$-O_{4e}>=2.430 Å, and < $Y_{1.5}Ce_{0.5}$-O,N_{8f}>=2.487 Å. At the 2c and 4e sites, N- distances are underbonded (6-5%) while the average O-distances are longer than expected (two of them are 6% more elongated and the other one 0.7-1.6% shorter than the predicted

values). At the 8f site, there are two distances shorter (3%) and two longer (10-11%) than the ideal values, and the overall size of the (Y,Ce)O,N_8 polyhedron is expanded with respect to the ideal values.

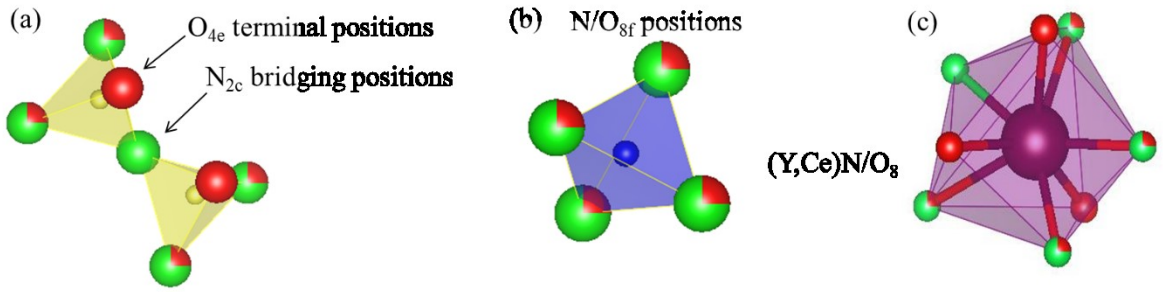

Figure 3. Polyhedral coordination environments of (a) $Si1_2(N,O)_7$ disilicate groups in yellow, (b) $Si2[(N/O)_{8f}]_4$ tetrahedra in blue and (c) $(Y,Ce)(N,O)_8$ in purple.

4. Discussion

The results of this study are in good agreement with a previously published refinement of $Y_2Si_3O_3N_4$ [14], although this reported N/O disorder over 2c and 8f anion sites whereas we find that the former is fully occupied by N. Our findings are also in agreement with first-principle calculations described in ref. [14]. This average anion distribution appears highly robust, as it is not changed by substitution of 25% of the Y^{3+} cations by Ce^{3+}. The anion site occupations are consistent with Pauling's second rule [19, 20] as the bond strength sums (of cation charge divided by coordination number) for the N-rich sites 2c and 8f sites (each coordinated by 2Si and 2Y/Ce) are 2.75, whereas O_{4e} (coordinated by 1Si and 3Y/Ce) has 2.125. The full occupancies of N_{2c} and O_{4e} sites, and exact 0.75/0.25 fractional occupancy of $(N/O)_{8f}$, suggest that the local anion arrangement in the latter sites is highly correlated. Previous studies of silicon and high valent transition metal oxynitrides have shown that covalency leads to uniform local coordination, so that in $Y_2Si_3O_3N_4$ the crystallographically observed average $Si2[(N/O)_{8f}]_4$ coordination with average composition $Si(N_{0.75}O_{0.25})_4$ corresponds to a tetrahedral SiN_3O group being present at all Si2 sites. Si1 is coordinated to one N_{2c} and O_{4e} and two $(N/O)_{8f}$ sites and so has average composition $SiNO(N_{0.75}O_{0.25})_2$, and thus a 1:1 mixture of SiN_3O and SiN_2O_2 groups are distributed over the Si1 positions.

The simplest structure to follow these coordination constraints is shown in Fig. 4 below, where O/N segregation leads to -Si2-O-Si1-N- chains in the [110] direction and -Si2-N-Si1-N- in the [$\bar{1}$10]. This would result in a monoclinic *Cm* supercell but no evidence for this is found in our diffraction data. This is likely because the $Si(N,O)_4$ tetrahedra can easily adopt a correlated disordered state as shown in Fig. 5. Applying the rules that each Si2 sits at the centre of an SiN_3O group, and each Si1 is coordinated to

either 2N or N+O (but never 2O) at the $(N/O)_{8f}$ sites, leads to configurations like those shown in Fig. 5b. The configurational entropy can be estimated using the approach in Pauling's famous ice rules paper [21]. 1 mol (N) of $Y_2Si_3O_3N_4$ contains 1 mol of Si2 sites, each of which has 4 allowed orientations of the SiN_3O tetrahedron, and the probability that an orientation is allowed by neighbouring tetrahedra is ¾ (to avoid O_{8f}-Si1-O_{8f} configurations). Hence the number of microstates is $W = (4.¾)^N$ and the residual molar entropy of $Y_2Si_3O_3N_4$ is predicted to be $S = k \ln W = R \ln 3$. It would be instructive to measure the entropy, but this is more difficult than for ice or magnetic analogues because the residual entropy is not frozen in directly below a phase transition.

The local Y(Ce) environment shown in Fig 3c contains one N_{2c}, three O_{4e}, and four $(N/O)_{8f}$ sites. Two of the $(N/O)_{8f}$ sites are bonded to the same Si1 and thus can be occupied by 2N or N+O (but not 2O). the other two are coordinated to different Si1's and so are uncorrelated. Hence, the Y(Ce) 8-coordination environment varies between N_5O_3 and N_2O_6 which is expected to broaden spectroscopic features from Ce^{3+} activator ions in this type of phosphor. There is no evidence for any Y/Ce ordering in our sample but electron diffraction could be used to check for possible short range ordering.

In conclusion, both $Y_2Si_3O_3N_4$ and the Ce-doped derivative $Y_{1.5}Ce_{0.5}Si_3O_3N_4$ are found to have highly segregated anion distributions, evidencing exclusively SiN_3O and SiN_2O_2 coordinations around Si, and local structural correlations between disordered $Si(N,O)_4$ tetrahedra that lead to an estimated residual entropy of $R \ln 3$. A broad range of N/O environments is found around 8-coordinate Y(Ce) sites which is expected to broaden their spectroscopic features.

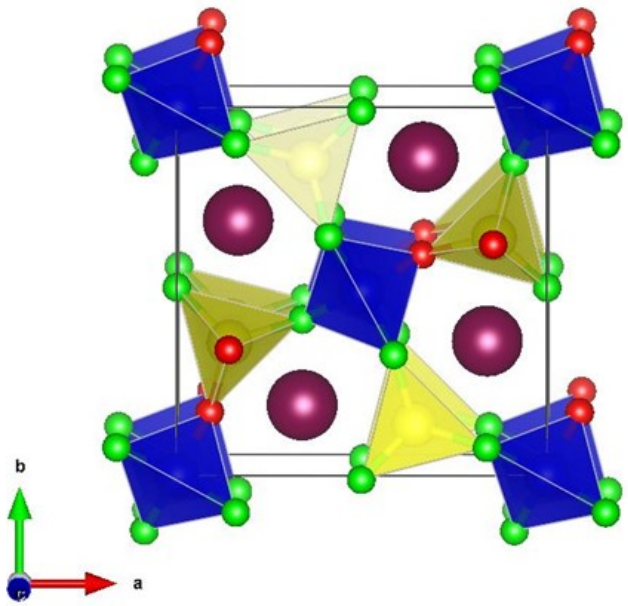

Figure 4. Schematic view of one example of the N/O distribution over the 8f sites.

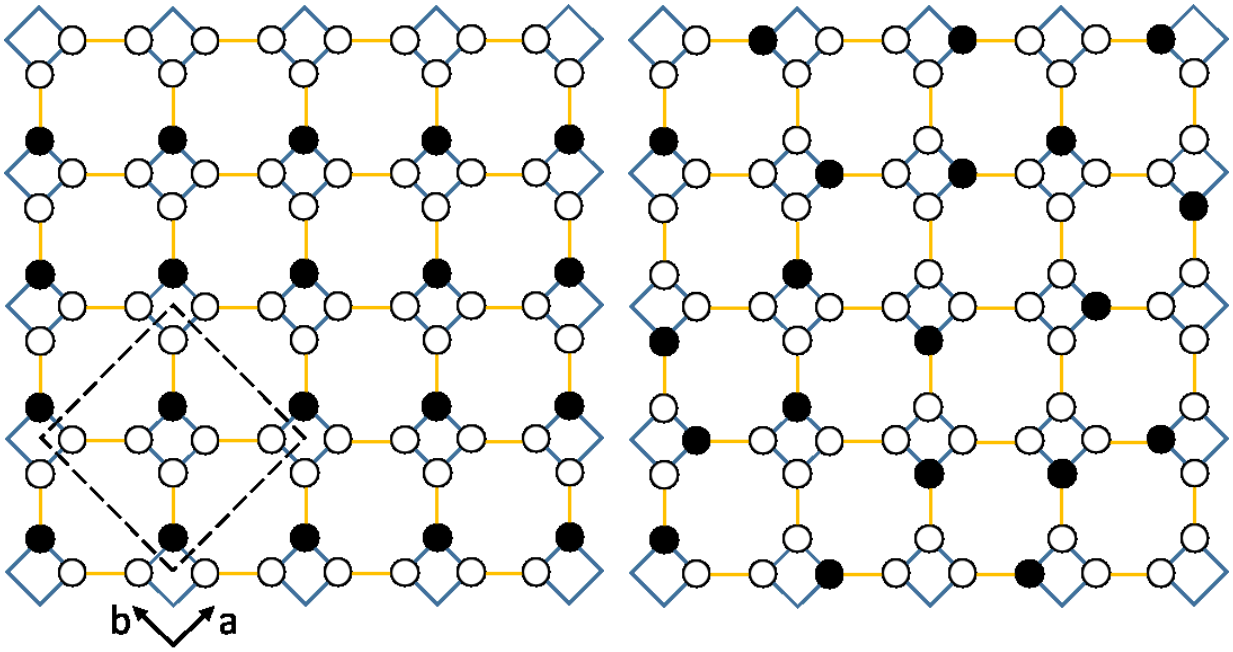

(a) (b)

Figure 5. Correlated anion order models for $Y_2Si_3O_3N_4$ with $(N/O)_{8f}$ atoms as white/black circles. $Si2N_3O$ groups are shown as blue squares, and pairs of $(N/O)_{8f}$ atoms connected to the same Si1 site are indicated by the yellow lines. (a) represents the simple long-range ordered model of Fig. 4, with unit cell shown. (b) shows a typical disordered configuration following the local coordination constraints.

Acknowledgments

This work was financially supported by EPSRC and the Ministry of Science and Technology in Taiwan (Contract No. MOST 107-2113-M-002-008-MY3) for RSL. We thank STFC for access to the ISIS facility.

References

[1] H. Kageyama, K. Hayashi, K. Maeda, J.P. Attfield, Z. Hiroi, J.M. Rondinelli, K.R. Poeppelmeier, Expanding frontiers in materials chemistry and physics with multiple anions, Nature Communications 9(1) (2018).
[2] M. Yang, J. Oró-Solée, J.A. Rodgers, A.B. Jorge, A. Fuertes, J.P. Attfield, Anion order in perovskite oxynitrides, Nature Chemistry 3(1) (2011) 47-52.
[3] J.P. Attfield, Principles and Applications of Anion Order in Solid Oxynitrides, Crystal Growth & Design, American Chemical Society, 2013, pp. 4623-4629.
[4] W.T. Chen, H.S. Sheu, R.S. Liu, J.P. Attfield, Cation-size-mismatch tuning of photoluminescence in oxynitride phosphors, J. Am. Chem. Soc. 134(19) (2012) 8022-8025.
[5] A.P. Black, K.A. Denault, J. Oró-Solé, A.R. Goñi, A. Fuertes, Red luminescence and ferromagnetism in europium oxynitridosilicates with a β-K_2SO_4 structure, Chem. Commun. 51(11) (2015) 2166-2169.

[6] R.-J. Xie, N. Hirosaki, Silicon-based oxynitride and nitride phosphors for white LEDs—A review, Science and Technology of Advanced Materials 8(7-8) (2007) 588-600.
[7] J.W.H. van Krevel, H.T. Hintzen, R. Metselaar, A. Meijerink, Long wavelength Ce^{3+} emission in Y–Si–O–N materials, J. Alloys Compd. 268(1) (1998) 272-277.
[8] S. Thomas, J. Oró-Solé, B. Glorieux, V. Jubera, V. Buissette, T. Le Mercier, A. Garcia, A. Fuertes, New luminescent rare earth activated oxynitridosilicates and oxynitridogermanates with the apatite structure, J. Mater. Chem. 22(45) (2012) 23913-23920.
[9] Y.Y. Ma, F. Xiao, S. Ye, Q.Y. Zhang, Characterization and luminescence properties of $Y_2Si_3O_3N_4$:Ce^{3+} phosphor for white light-emitting-diode, J. Electrochem. Soc. 159(4) (2012) H358-H362.
[10] J. Zhu, S. Qin, Z. Xia, Q. Liu, Synthesis and color-tunable emission studies of $Y_2Si_3O_3N_4$:Ce^{3+},Tb^{3+} phosphors, Ceramics International 41(10, Part A) (2015) 12633-12637.
[11] A. Koroglu, D.C. Apperley, R.K. Harris, D.P. Thompson, Oxygen–nitrogen ordering in yttrium nitrogen melilite, J. Mater. Chem. 6(6) (1996) 1031-1034.
[12] K.J.D. MacKenzie, G.J. Gainsford, M.J. Ryan, Rietveld refinement of the crystal structures of the yttrium silicon oxynitrides $Y_2Si_3N_4O_3$ (N-melilite) and $Y_4Si_2O_7N_2$ (J-phase), J. Eur. Ceram. Soc. 16(5) (1996) 553-560.
[13] R. Dupree, M.H. Lewis, M.E. Smith, High-resolution silicon-29 nuclear magnetic resonance in the Y-Si-O-N system, J. Am. Chem. Soc. 110(4) (1988) 1083-1087.
[14] C.M. Fang, G.A. de Wijs, R.A. de Groot, R. Metselaar, H.T. Hintzen, G. de With, O/N Ordering in $Y_2Si_3O_3N_4$ with the Melilite-type Structure from First-Principles Calculations, Chem. Mater. 12(4) (2000) 1071-1075.
[15] P.L. Wang, P.E. Werner, L. Gao, R.K. Harris, D.P. Thompson, Ordering of nitrogen and oxygen in nitrogen-containing melilites $Y_2Si_3O_3N_4$ and $Nd_2Si_{2.5}Al_{0.5}O_{3.5}N_{3.5}$, J. Mater. Chem. 7(10) (1997) 2127-2130.
[16] H. Rietveld, A profile refinement method for nuclear and magnetic structures, Journal of Applied Crystallography 2(2) (1969) 65-71.
[17] J. Rodríguez-Carvajal, Recent advances in magnetic structure determination by neutron powder diffraction, Physica B: Condensed Matter 192(1) (1993) 55-69.
[18] R. Shannon, Revised effective ionic radii and systematic studies of interatomic distances in halides and chalcogenides, Acta Crystallographica Section A 32(5) (1976) 751-767.
[19] L. Pauling, The principles determining the structure of complex ionic crystals, J. Am. Chem. Soc. 51(4) (1929) 1010-1026.
[20] A. Fuertes, Prediction of Anion Distributions Using Pauling's Second Rule, Inorganic Chemistry 45(24) (2006) 9640-9642.
[21] L. Pauling, The Structure and Entropy of Ice and of Other Crystals with Some Randomness of Atomic Arrangement, J. Am. Chem. Soc. 57(12) (1935) 2680-2684.